Theory of SNAP devices: basic equations and comparison with the experiment

M. Sumetsky*

OFS Laboratories, 19 Schoolhouse Road, Somerset, NJ 08873, USA

*sumetski@ofsoptics.com

Abstract: A SNAP (Surface Nanoscale Axial Photonics) device consists of an optical fiber with introduced nanoscale effective radius variation, which is coupled to transverse input/output waveguides. The input waveguides excite whispering gallery modes circulating near the fiber surface and slowly propagating along the fiber axis. In this paper, the theory of SNAP devices is developed and applied to the analysis of transmission amplitudes of simplest SNAP models exhibiting a variety of asymmetric Fano resonances and also to the experimental characterization of a SNAP bottle microresonator and to a chain of 10 coupled microresonators. Excellent agreement between the theory and the experiment is demonstrated.

OCIS codes: (060.2340) Fiber optic component; (140.3945) Microcavities; (230.3990) Micro-optic device.

References and links

1. M. Sumetsky, "Localization of light in an optical fiber with nanoscale radius variation," in CLEO/Europe and EQEC 2011 Conference Digest, postdeadline paper PDA_8.
2. M. Sumetsky and J. M. Fini, "Surface nanoscale axial photonics," Opt. Express **19**(27), 26470–26485 (2011).
3. M. Sumetsky, D. J. DiGiovanni, Y. Dulashko, J. M. Fini, X. Liu, E. M. Monberg, and T. F. Taunay, "Surface nanoscale axial photonics: robust fabrication of high-quality-factor microresonators," Opt. Lett. **36**(24), 4824–4826 (2011).
4. M. Sumetsky, K. Abedin, D. J. DiGiovanni, Y. Dulashko, J. M. Fini, E. Monberg, and E. M. Monberg, "Coupled high Q-factor surface nanoscale axial photonics (SNAP) microresonators," Opt. Lett. **37**(6), 990–992 (2012).
5. M. Wilson, "Optical fiber microcavities reach angstrom-scale precision," Phys. Today **65**(2), 14–16 (2012).
6. M. Sumetsky, D. J. DiGiovanni, Y. Dulashko, X. Liu, E. M. Monberg, and T. F. Taunay, "Photo-induced SNAP: fabrication, trimming, and tuning of microresonator chains," Opt. Express **20**(10), 10684–10691 (2012).
7. F. Luan, E. Magi, T. Gong, I. Kabakova, and B. J. Eggleton, "Photoinduced whispering gallery mode microcavity resonator in a chalcogenide microfiber," Opt. Lett. **36**(24), 4761–4763 (2011).
8. H. G. Limberger, P.-Y. Fonjallaz, R. P. Salathé, and F. Cochet, "Compaction- and photoelastic-induced index changes in fiber Bragg gratings," Appl. Phys. Lett. **68**(22), 3069–3071 (1996).
9. A. D. Yablon, M. F. Yan, P. Wisk, F. V. DiMarcello, J. W. Fleming, W. A. Reed, E. M. Monberg, D. J. DiGiovanni, J. Jasapara, and M. E. Lines, "Refractive index perturbations in optical fibers resulting from frozen-in viscoelasticity," Appl. Phys. Lett. **84**(1), 19–21 (2004).
10. A. D. Stone and A. Szafer, "What is measured when you measure a resistance?-The Landauer formula revisited," IBM J. Res. Develop. **32**(3), 384–413 (1988).
11. H. U. Baranger, R. A. Jalabert, and A. D. Stone, "Quantum-chaotic scattering effects in semiconductor microstructures," Chaos **3**(4), 665–682 (1993).
12. S. Datta, *Electronic Transport in Mesoscopic Systems* (Cambridge University Press, UK, 1997).
13. F.-M. Dittes, "The decay of quantum systems with a small number of open channels," Phys. Rep. **339**(4), 215–316 (2000).
14. S. Fan, P. R. Villeneuve, J. D. Joannopoulos, M. Khan, C. Manolatou, and H. Haus, "Theoretical analysis of channel drop tunneling processes," Phys. Rev. B **59**(24), 15882–15892 (1999).
15. Y. Xu, Y. Li, R. K. Lee, and A. Yariv, "Scattering-theory analysis of waveguide-resonator coupling," Phys. Rev. E Stat. Phys. Plasmas Fluids Relat. Interdiscip. Topics **62**(5), 7389–7404 (2000).
16. M. Sumetsky and B. Eggleton, "Modeling and optimization of complex photonic resonant cavity circuits," Opt. Express **11**(4), 381–391 (2003).
17. S. Albeverio, F. Gesztesy, R. Høegh-Krohn, and H. Holden, *Solvable Models in Quantum Mechanics* (American Mathematical Society, Providence, 2004).
18. Yu. N. Demkov and V. N. Ostrovskii, *Zero-Range Potentials and their Applications in Atomic Physics* (Plenum, New York, 1988).

#174047 - $15.00 USD Received 8 Aug 2012; revised 11 Sep 2012; accepted 12 Sep 2012; published 17 Sep 2012

19. M. Sumetsky, "Whispering-gallery-bottle microcavities: the three-dimensional etalon," Opt. Lett. **29**(1), 8–10 (2004).
20. S. M. Spillane, T. J. Kippenberg, O. J. Painter, and K. J. Vahala, "Ideality in a fiber-taper-coupled microresonator system for application to cavity quantum electrodynamics," Phys. Rev. Lett. **91**(4), 043902 (2003).
21. A. E. Miroshnichenko, S. Flach, and Yu. S. Kivshar, "Fano resonances in nanoscale structures," Rev. Mod. Phys. **82**(3), 2257–2298 (2010).
22. T. A. Birks, J. C. Knight, and T. E. Dimmick, "High-resolution measurement of the fiber diameter variations using whispering gallery modes and no optical alignment," IEEE Photon. Technol. Lett. **12**(2), 182–183 (2000).
23. M. Sumetsky and Y. Dulashko, "Radius variation of optical fibers with angstrom accuracy," Opt. Lett. **35**(23), 4006–4008 (2010).
24. J. Ziman, *Elements of Advanced Quantum Theory* (Cambridge University Press, London, 1969).

1. Introduction

Surface nanoscale axial photonics (SNAP), the record accurate and low loss platform for fabrication of complex miniature photonic circuits, was introduced and described in the series of recent publications [1–6]. A SNAP device is illustrated in Fig. 1. It consists of an optical fiber with specially introduced nanometer-scale radius variation, called the SNAP fiber (SF), and transverse input/output waveguides coupled to this fiber. The waveguides are usually fabricated of a biconical fiber with micron-scale diameter waist, or, alternatively, can be planar waveguides fabricated lithographically. The input waveguide launches whispering gallery modes (WGMs), which circulate near the SF surface and experience slow propagation along the fiber axis. In SNAP, the WGMs have very small propagation constant and, for this reason, are sensitive to dramatically small nanoscale variation of the fiber radius and similar variation of the refractive index [1,6,7]. This enables fabrication of complex SNAP circuits (consisting, e.g., of long series of coupled microresonators) with record high accuracy and record small optical losses [3–6]. The performance of SNAP devices depends only on the effective radius variation of the fiber, which combines the contributions of variations of the fiber physical radius and its refractive index. For nanoscale variations, these contributions usually have the same order of magnitude [8,9].

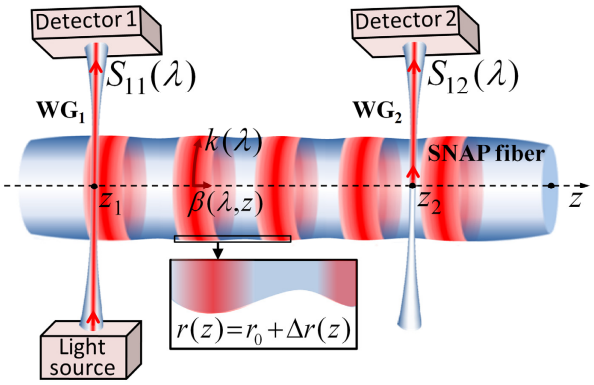

Fig. 1. Illustration of a SNAP device. Red: WGM microresonators. WG1 and WG2 are the waveguide 1 and waveguide 2 coupled to the SF. Inset: magnified nanometer-scale fiber radius variation.

The goal of this paper is to develop the theory which can be directly applied both to modeling of SNAP devices and to their evaluation from the experimental data. The results obtained are essentially based on the previous work [1,2] where the one-dimensional Schrödinger equation governing the slow propagation of WGMs along the fiber with nanoscale effective radius variation was derived. This equation is described in Section 2. In [1,2], the transmission amplitude of a SNAP device was expressed through the Green's function of the Schrödinger equation which is supposed to be renormalized to take into account the losses due to coupling to the waveguide. However, the actual application of the

#174047 - $15.00 USD Received 8 Aug 2012; revised 11 Sep 2012; accepted 12 Sep 2012; published 17 Sep 2012

theory [1,2] was limited because the problem of renormalization has not been addressed. The theory developed in Section 3 solves this problem. In addition, Section 3 includes the case of an SF coupled to several waveguides. It is shown that the transmission amplitudes of a SNAP device coupled to N waveguides, one of which is the input/output waveguide and others are the output waveguides, can be expressed through the solution of the one-dimensional Schrödinger equation of Refs [1,2]. and $3N$ complex constants, which determine the lossy SF/waveguide coupling. In the case of lossless coupling, the number of constants is reduced to N. In Section 4, the developed theory is applied to the investigation of transmission amplitudes through a localized state and also through a uniform SF coupled to one waveguide, which exhibits a variety of asymmetric Fano resonances. In Section 5, it is shown that sharp transmission resonances can characterize a lossy SNAP device coupled to two waveguides. In Section 6, the experimental characterization of the SNAP bottle microresonator and of a chain of 10 coupled microresonators is demonstrated to be in the excellent agreement with the developed theory. It is shown that the effective radius variation of a SNAP fiber and all of the transmission amplitude parameters can be accurately determined from the experiment. The results of this paper are discussed and summarized in Section 7.

2. WGMs in a SNAP fiber in the absence of input/output waveguides

The field distribution of a WGM *adiabatically* propagating along the axis z of an SF with *nanoscale* smooth radius variation (and/or equivalent refractive index variation) *in the absence of input/output waveguides* is defined as

$$U_{m,p,q}(\mathbf{r}) = \Psi_{m,p,q}(z)\Xi_{m,p}(\rho)\exp(im\varphi) \tag{1}$$

where (z,ρ,φ) are the cylindrical coordinates, m is the discrete azimuthal quantum number, p is the discrete radial quantum number, and q is the discrete or continuous axial quantum number. Function $\Psi_{m,p,q}(z)$ determines the axial distribution of the WGM and satisfies the one-dimensional Schrödinger equation [1,2]:

$$\frac{d^2\Psi}{dz^2} + \beta^2(\lambda,z)\Psi = 0, \qquad \beta^2(\lambda,z) = E(\lambda) - V(z). \tag{2}$$

In this equation, the energy is proportional to the variation of radiation wavelength λ and the potential is proportional to the fiber radius variation $\Delta r(z) = r(z) - r_0$ and refractive index variation $\Delta n_f(z) = n_f(z) - n_{f0}$:

$$\begin{gathered} E(\lambda) = -2k^2(\lambda_{res})\frac{\lambda - \lambda_{res} - i\gamma_{res}}{\lambda_{res}}, \qquad V(z) = -2k^2(\lambda_{res})\frac{\Delta r_{eff}(z)}{r_0}, \\ \frac{\Delta r_{eff}(z)}{r_0} = \frac{\Delta r(z)}{r_0} + \frac{\Delta n_f(z)}{n_{f0}}, \quad k(\lambda_{res}) = \frac{2\pi n_{f0}}{\lambda_{res}}. \end{gathered} \tag{3}$$

The joint contribution of the fiber radius and refractive index variation is expressed in Eqs. (2) and (3) only through the effective radius variation $\Delta r_{eff}(z)$. In silica, the attenuation parameter γ_{res} is very small (typically, $\gamma_{res} < 0.1\,\text{pm}$). The resonance wavelength λ_{res} coincides with the transverse eigenvalue λ_{mp} corresponding to the zero propagation constant, i.e., to the zero axial speed of light. Equation (2) is valid for wavelengths λ in a small neighborhood of $\lambda_{res} = \lambda_{mp}$ with the fixed quantum numbers m and p. These numbers are omitted below for brevity.

#174047 - $15.00 USD Received 8 Aug 2012; revised 11 Sep 2012; accepted 12 Sep 2012; published 17 Sep 2012

3. Theory of a SNAP device

It is instructive to recall the general theory of transmission through waveguides coupled to a complex-shaped cavity. The latter has been of significant interest in the last few decades both in quantum mechanics and optics [10–16]. The important problem that has been addressed in this theory was the elucidation of the relation between the transmission amplitudes through the waveguides and the Green's function of the isolated cavity. To solve this problem, the *renormalized Green's function* of the cavity was introduced. This function modifies the Green's function of the isolated cavity (i.e., the cavity uncoupled from the waveguides) called the *bare Green's function*, and takes into account the losses due to coupling to the waveguides. It was found that the transmission amplitudes through the waveguides can be expressed through the overlap integrals between the renormalized Green's function and the travelling waves propagating along the waveguides.

The major challenge of the theory of non-one-dimensional cavities coupled to waveguides is the actual determination of the renormalized Green's function for a given cavity shape [10–15]. This problem has been addressed in several special cases only. For example, for quantum mechanical and optical billiards, this problem was approached in the semiclassical approximation [11]. For a cavity assembled of several weakly coupling elementary cavities, this problem was considered in the tight-binding approximation [16]. Besides, the behavior of non-one-dimensional cavities can be qualitatively analyzed with the quantum graph theory [17].

Crucially, it is shown in this paper that in many cases the relation between the bare Green's function and renormalized Green's function of a SNAP device can be found analytically. For the considered slow axial propagation of light, i.e., when the radiation wavelength is close to the resonance λ_{res}, the bare 3D Green's function of the SNAP device is expressed through the 1D Green's function $G(\lambda, z_1, z_2)$ of Eq. (2) (see Appendix 1). Similarly, the renormalized 3D Green's function is expressed through the 1D renormalized Green's function $\bar{G}(\lambda, z_1, z_2)$ defined below. Finally, the transmission amplitudes through the waveguides are simply expressed through the Green's function $\bar{G}(\lambda, z_1, z_2)$.

Consider an SF coupled to N transverse waveguides WG_1, WG_2, …, WG_N. Assume that WG_1 serves as the input and output waveguide while all other waveguides are the output waveguides only (in Fig. 1, $N = 2$). Then, the renormalized Green's function of the SF, $\bar{G}(\lambda, z, z_1)$, is determined as the Green's function of equation:

$$\frac{d^2\Psi(z)}{dz^2} + \left[\beta^2(\lambda, z) + \sum_{n=1}^{N} D_n \delta(z - z_n) \right] \Psi(z) = 0. \tag{4}$$

This equation coincides with Eq. (2) for $D_n = 0$. The real part of D_n determines the phase shift due to coupling to WG_n while its imaginary part takes into account the radiation loss through WG_n, In Eq. (4), coupling to waveguides WG_n is modeled with *zero-range potentials* $D_n \delta(z - z_n)$ [17,18], which is justified if the waveguide width is much smaller than the WGM axial wavelength. The latter assumption is in agreement with the experiment, where, typically, the microfiber diameter is ~1 μm and the axial wavelength is greater than 10 μm. Under the same assumptions, the transmission amplitude through WG_1 is simply found as (Appendix 1)

$$S_{11}(\lambda) = S_{11}^{(0)} - i \,|\, C_1 \,|^2 \, \bar{G}(\lambda, z_1, z_1), \tag{5}$$

and the transmission amplitude from WG_1 to WG_n is

$$S_{1n}(\lambda) = S_{1n}^{(0)} - i C_1 C_n^* \bar{G}(\lambda, z_1, z_n), \tag{6}$$

#174047 - $15.00 USD Received 8 Aug 2012; revised 11 Sep 2012; accepted 12 Sep 2012; published 17 Sep 2012

where constants C_n are the SF/WG$_n$ coupling parameters and $S_{1n}^{(0)}$ are the non-resonant components of the transmission amplitudes S_{1n}. These parameters are slow functions of wavelength and can be set to constants in the considered neighborhood of resonance λ_{res}.

Equation (4) for the renormalized Green's function together with Eqs. (5) and (6) express the transmission amplitudes through the effective radius variation of the SF and 3N complex constants $S_{1n}^{(0)}$, C_n, and D_n. These equations are applied below to the analysis of basic theoretical models and to the treatment of experimental data.

4. Transmission amplitude of a SNAP device coupled to a single waveguide

For a single waveguide WG$_1$ coupled to an SF ($N=1$) the renormalized Green's function $\bar{G}(\lambda, z_1, z_2)$ of Eq. (4) is expressed through the bare Green's function $G(\lambda, z_1, z_2)$ of Eq. (2) as (see Appendix 2):

$$\bar{G}(\lambda, z_1, z_2) = \frac{G(\lambda, z_1, z_2)}{1 + D_1 G(\lambda, z_1, z_1)}. \tag{7}$$

Substitution of Eq. (7) into Eq. (5) yields:

$$S_{11}(\lambda) = S_{11}^{(0)} - \frac{i\,|C_1|^2\, G(\lambda, z_1, z_1)}{1 + D_1 G(\lambda, z_1, z_1)}. \tag{8}$$

In the case of lossless resonant transmission, $G(\lambda, z_1, z_2)$ is real (e.g., as in a lossless bottle resonator [19]), and, due to energy conservation, the absolute value of the transmission amplitude defined by Eq. (5) equals unity, $|S_{11}(\lambda)| \equiv 1$ for all real $G(\lambda, z_1, z_2)$. The latter equation immediately leads to $S_{11}^{(0)} = 1$ and $\mathrm{Im}\, D_1 = |C_1|^2/2$. As a result, for lossless resonant coupling and any SF profile, which not necessarily corresponds to the real-valued $G(\lambda, z_1, z_2)$ (i.e., the WGM propagation can be lossy and delocalized),

$$S_{11}(\lambda) = \frac{1 + \left(\mathrm{Re}\, D_1 - \frac{i}{2}|C_1|^2\right) G(\lambda, z_1, z_1)}{1 + \left(\mathrm{Re}\, D_1 + \frac{i}{2}|C_1|^2\right) G(\lambda, z_1, z_1)}. \tag{9}$$

From the energy conservation law, the absolute value of the transmission amplitude defined by Eq. (9) is always less than unity. This can be verified using the known inequality $\mathrm{Im}\, G(\lambda, z_1, z_1) < 0$ [12]. The case of lossless resonant coupling described by Eq. (9) is often referred to as *ideal coupling* which is confirmed experimentally for weak coupling and a single mode waveguide [20]. For an SF ideally coupled to N waveguides, $S_{11}^{(0)} = 1$, $S_{1n}^{(0)} = 0$, and $\mathrm{Im}\, D_n = |C_n|^2/2$.

For lossy coupling, the energy conservation law implies $|S_{11}(\lambda)| < 1$, which restricts the possible values of $S_{11}^{(0)}$, C_1, and D_1 by the inequalities (Appendix 3):

$$|S_{11}^{(0)}| < 1, \tag{10}$$

$$\mathrm{Im}(D_1) > |C_1|^2 \frac{1 - \mathrm{Re}(S_{11}^{(0)})}{1 - |S_{11}^{(0)}|^2}. \tag{11}$$

These inequalities are useful in the modeling of SNAP devices as well as in the numerical treatment of experimental data.

#174047 - $15.00 USD Received 8 Aug 2012; revised 11 Sep 2012; accepted 12 Sep 2012; published 17 Sep 2012

4.1. Transmission through localized states of an SF

Consider a fully localized SNAP bottle microresonator [19] with a real-valued axial distribution of eigenmode $\Psi_n(z)$ having the energy eigenvalue E_n. The Green's function of Eq. (2) near E_n is [12]

$$G(\lambda, z_1, z_2) = \frac{\Psi_n(z_1)\Psi_n(z_2)}{E(\lambda) - E_n + i\Gamma_0}, \tag{12}$$

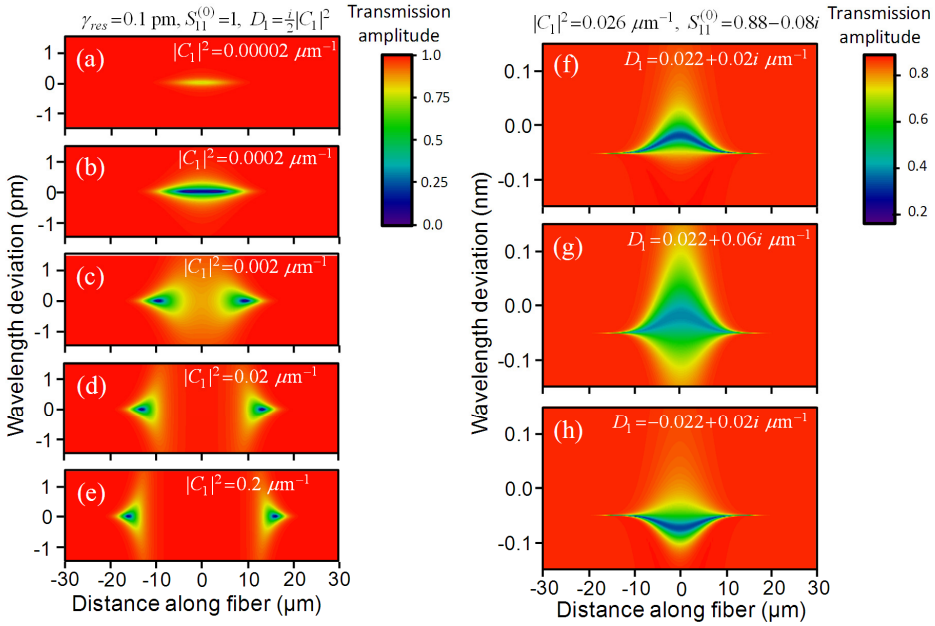

Fig. 2. Surface plots of the transmission amplitude as a function of distance along the fiber and wavelength deviation for λ = 1.5 μm, γ_{res} = 0.1 pm, n_{f0} = 1.5, and different coupling parameters shown on the plots.

where $\Gamma_0 = (8\pi^2 n_{f0}^2 / \lambda_{res}^3)\gamma_{res}$ is the width of resonance due to the propagation losses in the SF. Substitution of Eq. (12) into Eq. (8) yields the Fano formula [21] for the transmission amplitude:

$$S_{11}(\lambda) = S_{11}^{(0)} - \frac{i\Lambda_n}{(E(\lambda) - E_n - \Delta_n) + i(\Gamma_0 + \Sigma_n)}, \tag{13}$$
$$\Lambda_n = |C_1|^2 \Psi_n^2(z_1), \qquad \Delta_n = -\mathrm{Re}(D_1)\Psi_n^2(z_1), \qquad \Sigma_n = \mathrm{Im}(D_1)\Psi_n^2(z_1).$$

Thus, coupling to the transverse WG_1 replaces the resonance width Γ_0 with $\Gamma_n = \Gamma_0 + \Sigma_n$, where the self-energy Σ_n is proportional to $\mathrm{Im}(D_1)$ and describes additional losses due to leakage into the waveguide [12], and also shifts the resonance position by Δ_n, which is proportional to $\mathrm{Re}(D_1)$. The self-energy term Σ_n is also proportional to the intensity of WGM $\Psi_n(z)$ at position z_1 of WG_1 [2]. In particular, Σ_n vanishes at the WGM nodes (here $\Lambda_n = 0$ and the resonant WGM is uncoupled from the waveguide and, hence, is invisible or dark). Alternatively, the largest coupling to the microfiber is achieved at the WGM antinodes.

In the case of lossless coupling Eqs. (9) and (12) yield:

#174047 - $15.00 USD Received 8 Aug 2012; revised 11 Sep 2012; accepted 12 Sep 2012; published 17 Sep 2012

$$S_{11}(\lambda) = \frac{(E(\lambda) - E_n - \Delta_n) + i(\Gamma_0 - \frac{1}{2}\Lambda_n)}{(E(\lambda) - E_n - \Delta_n) + i(\Gamma_0 + \frac{1}{2}\Lambda_n)}, \tag{14}$$

Equation (14) is the well-known Breit-Wigner resonance representation of the scattering amplitude [12].

The wavelength/spatial dependence in the neighborhood of a localized state can be elucidated by considering the characteristic fundamental state of a harmonic oscillator with Gaussian spatial mode distribution $\Psi_0(z) = (2/\pi)^{1/4} z_w^{-1/2} \exp[-(z/z_w)^2]$. For example, in the case of lossless coupling Eq. (14) yields the following wavelength/spatial dependence of the transmission amplitude:

$$S_{11}(\lambda) = \frac{(\lambda - \lambda_{res}) - i(\gamma_{res} - \gamma_C \exp[-(z/z_w)^2])}{(\lambda - \lambda_{res}) - i(\gamma_{res} + \gamma_C \exp[-(z/z_w)^2])}, \tag{15}$$

where $\gamma_C = (2\pi)^{-5/2} \lambda_{res}^3 n_{f0}^{-2} z_w^{-1} |C_1|^2$.

Figure 2 shows the surface plots of the transmission amplitude $|S_{11}(\lambda)|$ as a function of distance along the fiber and wavelength deviation for $\lambda_{res} = 1.5\,\mu$m, $\gamma_{res} = 0.1$ pm, and $n_{f0} = 1.5$. The axial FWHM of the mode is set to to 20 μm, which corresponds to $z_w = 12\,\mu$m. In Fig. 2(a)-2(e) the plots of transmission amplitude for ideal lossless coupling ($S_{11}^{(0)} = 1$, $D_1 = i|C_1|^2/2$) are shown. It is seen that the resonance width grows approaching the WGM maxima. For relatively small coupling, the surface plot has a single maximum. For larger coupling, the spatial behavior of the transmission amplitude splits into two peaks indicating the condition of critical coupling. Next, the parameters $|C_1|^2 = 0.026\,\mu\text{m}^{-1}$, $D_1 = 0.022 + 0.02i\,\mu\text{m}^{-1}$, and $S_{11}^{(0)} = 0.88 - 0.08i$ of Fig. 2(f) correspond to the lossy transmission amplitudes of the SNAP bottle microresonator considered in Section 6. In this case, the value of internal losses in the SF, γ_{res}, is no longer important because its contribution is much smaller than the contribution of losses due to scattering into other WGMs and into continuum. It is seen that the scattering losses result in dramatic growth of the resonance widths compared to those in Fig. 2(a)-2(e). In addition, the lossy coupling leads to the asymmetric resonances indicating the Fano effect [21]. For comparison, Fig. 2(g) shows the situation with scattering parameters similar to those in Fig. 2(f) except for the increased value of output losses (determined by the imaginary part of D_1) $D_1 = 0.022 + 0.06i\,\mu\text{m}^{-1}$. Finally, the surface plot of Fig. 2(h) corresponds to the same parameters as those in Fig. 2(f) except for the opposite coupling phase shift (determined by the real part of D_1), $D_1 = -0.022 + 0.02i\,\mu\text{m}^{-1}$. In the latter case the asymmetric incline of spectral resonances is opposite to that in Fig. 2(f).

For a larger number of discrete SF resonances,

$$G(\lambda, z_1, z_1) = \sum_n \frac{|\Psi_n(z_1)|^2}{E(\lambda) - E_n + i\Gamma_n} \tag{16}$$

and the generalization of Eqs. (13) and (16) is straightforward.

4.2. Transmission through a uniform SF

In the case of a uniform SF, the bare Green's function is

#174047 - $15.00 USD Received 8 Aug 2012; revised 11 Sep 2012; accepted 12 Sep 2012; published 17 Sep 2012

$$G(\lambda, z_1, z_2) = \frac{\exp[i(E(\lambda) - E_0 + i\Gamma_0)^{1/2} \mid z_2 - z_1 \mid]}{2i(E(\lambda) - E_0 + i\Gamma_0)^{1/2}}. \qquad (17)$$

The surface plots of the transmission amplitude $|S_{11}(\lambda)|$ in Fig. 3 as a function of wavelength deviation and coupling parameters are found from Eqs. (8) and (17) for $\lambda_{res} = 1.5\,\mu$m, $\gamma_{res} = 0.1$ pm, $n_{f0} = 1.5$. The surface plots of the lossless transmission amplitude are shown in Fig. 3(a) and 3(b). In Fig. 3(a), $\mathrm{Re}(D_1) = 0$, i.e., coupling between the SF and the WG_1 does not cause a phase shift. In the presence of a phase shift, the behavior of the transmission amplitude can be more complex. This is illustrated in Fig. 3(b) for $\mathrm{Re}(D_1) = 2\,\mathrm{Im}(D_1)$. Fig. 3(c) shows the surface plot of the lossy transmission amplitude calculated for $S_{11}^{(0)} = 0.88 - 0.08i$ taken from the experiment of Section 6 and the ratio of coupling parameters D_1 and $|C_1|^2$ from the same experiment. For comparison, Fig. 3(d) shows the behavior of the transmission amplitude with the same parameters as in Fig. 3(c) except for the twice greater values of $\mathrm{Re}(D_1)$.

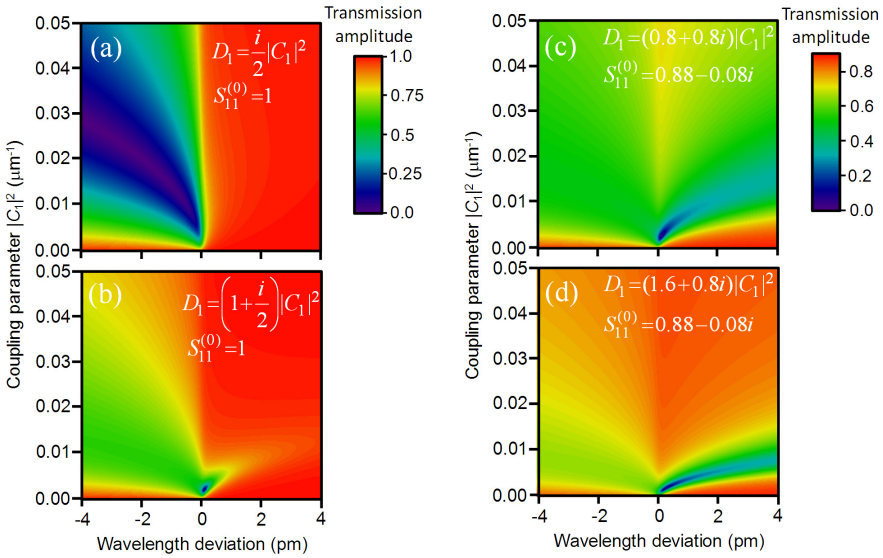

Fig. 3. Surface plot of the transmission amplitude through a uniform SF as a function of wavelength deviation and coupling parameters. (a), (b) – lossless transmission (b),(c) – lossy transmission. The SF parameters are λ = 1.5 μm, γ_{res} = 0.1 pm, and n_{f0} = 1.5. Other parameters are given in this Fig. 3.

5. Transmission amplitudes of a SNAP device coupled to two waveguides

Equation (8) shows that the transmission amplitude can be expressed as a rational function of the coupling parameters C_1, D_1, and the bare Green's function of the SF $G(\lambda, z_1, z_1)$. Similarly, it would appear reasonable that for a SNAP device coupled to several waveguides, WG_1, WG_2, …, WG_N, i.e., the transmission amplitudes $S_{1n}(\lambda)$ are the rational functions of the coupling parameters C_n, D_n, and the values of Green's function $G(\lambda, z_{n_1}, z_{n_2})$ calculated at the waveguide positions z_{n_1} and z_{n_2}, $n_1, n_2 = 1, 2, ..., N$. In this Section, this result is demonstrated for a SNAP device coupled to two waveguides (Fig. 1). The transmission amplitude of light entering and exiting WG_1, $S_{11}(\lambda)$, and the transmission amplitude of light

#174047 - $15.00 USD Received 8 Aug 2012; revised 11 Sep 2012; accepted 12 Sep 2012; published 17 Sep 2012

entering WG_1 and exiting WG_2, $S_{12}(\lambda)$, are determined from Eq. (5) and Eq. (6) for $N=2$. The values of renormalized Green's function $\bar{G}(\lambda,z_1,z_1)$ and $\bar{G}(\lambda,z_1,z_2)$ in these equations are expressed through the coupling parameters C_1,C_2,D_1,D_2, and the values of the bare Green's function $G(\lambda,z_1,z_1)$ and $G(\lambda,z_1,z_2)$ as (Appendix 2):

$$\bar{G}(\lambda,z_1,z_1)=\frac{G(\lambda,z_1,z_1)+D_2\left(G(\lambda,z_1,z_1)G(\lambda,z_2,z_2)-G^2(\lambda,z_1,z_2)\right)}{\left(1+D_1G(\lambda,z_1,z_1)\right)\left(1+D_2G(\lambda,z_2,z_2)\right)-D_1D_2G^2(\lambda,z_1,z_2)}, \quad (18)$$

$$\bar{G}(\lambda,z_1,z_2)=\frac{G(\lambda,z_1,z_2)}{\left(1+D_1G(\lambda,z_1,z_1)\right)\left(1+D_2G(\lambda,z_2,z_2)\right)-D_1D_2G^2(\lambda,z_1,z_2)}, \quad (19)$$

where, as noted in Section 4, in the case of lossless coupling,

$$\mathrm{Im}\,D_n=\tfrac{1}{2}|C_n|^2. \quad (20)$$

5.1. Transmission through the localized states of an SF

Near a separated resonance, the bare Green's function is defined by Eq. (12). Then Eqs. (5), (6), (18) and (19) for the lossless coupling are simplified:

$$S_{11}(\lambda)=\frac{E(\lambda)-E_n+\Delta_n+i\left(\Gamma_0+\Sigma_n^{(2)}-\Sigma_n^{(1)}\right)}{E(\lambda)-E_n+\Delta_n+i\left(\Gamma_0+\Sigma_n^{(2)}+\Sigma_n^{(1)}\right)}, \quad (21)$$

$$S_{12}(\lambda)=\frac{-2i\Xi_n}{E(\lambda)-E_n+\Delta_n+i\left(\Gamma_0+\Sigma_n^{(1)}+\Sigma_n^{(2)}\right)}, \quad (22)$$

$$\Sigma_n^{(j)}=\tfrac{1}{2}|C_j|^2\,\Psi_n^2(z_j),\qquad \Xi_n=C_1C_2^*\Psi_n(z_1)\Psi_n(z_2),\qquad \Delta_n=\mathrm{Re}(D_1)\Psi_n^2(z_1)+\mathrm{Re}(D_2)\Psi_n^2(z_2). \quad (23)$$

Equation (21) is similar to Eq. (14) found for a SNAP device coupled to a single waveguide where the internal losses Γ_0 are replaced with $\Gamma_0+\Sigma_n^{(2)}$, taking into account the leakage through WG_2. Thus, the presence of the second waveguide modifies the widths and shifts of the individual resonances (e.g., those in a bottle microresonator); however, it does introduce qualitative changes in the spectral behavior.

5.2. Transmission through a uniform SF

If the coupling to WG_2 is negligible then the renormalized Green's function defined by Eqs. (18) and (19) coincides with that of a single waveguide device defined by Eq. (7). Here we consider the opposite case of large coupling to WG_2. Then, for the lossless coupling to WG_1, i.e., for $S_{11}^{(0)}=1$, $D_2=\infty$, and $D_1=\mathrm{Re}(D_1)+\frac{i}{2}|C_n|^2$, Eqs. (5), (18), and (20) yield

$$S_{11}(\lambda)=\frac{G(\lambda,z_2,z_2)-(\mathrm{Re}\,D_1-\frac{i}{2}|C_1|^2)\left(G(\lambda,z_1,z_1)G(\lambda,z_2,z_2)-G^2(\lambda,z_1,z_2)\right)}{G(\lambda,z_2,z_2)-(\mathrm{Re}\,D_1+\frac{i}{2}|C_1|^2)\left(G(\lambda,z_1,z_1)G(\lambda,z_2,z_2)-G^2(\lambda,z_1,z_2)\right)}. \quad (24)$$

Figure 4 shows the surface plots of the absolute value of the transmission amplitude found from this equation for the uniform SF, when the bare Green's function is defined by Eq. (17). In Fig. 4(a), it is assumed that $\mathrm{Re}(D_1)=0$, i.e., that coupling to WG_1 does not shift the resonances. To understand the effect of shifting, Fig. 4(b) shows the case when $\mathrm{Re}(D_1)=2\,\mathrm{Im}(D_1)$. Fig. 4(a) shows that the zero phase shift corresponds to symmetric

#174047 - $15.00 USD Received 8 Aug 2012; revised 11 Sep 2012; accepted 12 Sep 2012; published 17 Sep 2012

resonance peaks, while, according to Fig. 4(b), the shapes of resonances become asymmetric when the real and imaginary parts of D_1 are comparable. The interesting feature of spectra in Fig. 4 is the narrow transmission resonances appearing due to the interference between WGMs reflected from WG_1 and WG_2. The widths of these resonances are proportional to $1/|C_1|^2$ and become very small with the growth of SF/MF_1 coupling.

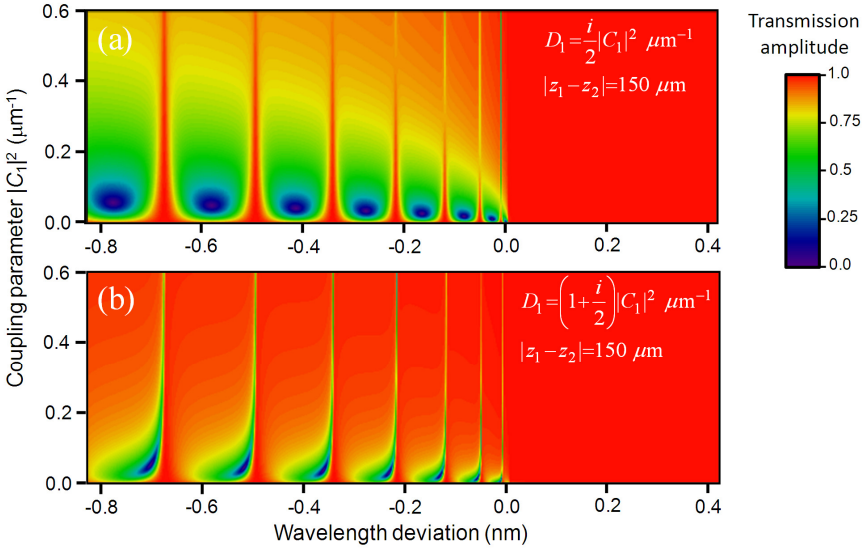

Fig. 4. Surface plots of the transmission amplitude $S_{11}(\lambda)$ through a uniform SF coupled to two waveguides, WG_1 and WG_2, as a function of wavelength deviation and the coupling parameter $|C_1|^2$ to WG_1. Coupling to WG_2 is assumed to be large compared to coupling to WG_1. The waveguides are spaced by 150 μm. (a) – $D_1 = i|C_1|^2/2$ (b) – $D_1 = (1 + i/2)|C_1|^2$. The SF parameters are $\lambda = 1.5$ μm, $\gamma_{res} = 0.1$ pm, and $n_{f0} = 1.5$.

6. A SNAP bottle microresonator and a chain of 10 coupled microresonators: theory vs. experiment

Experimentally, SNAP bottle microresonators are fabricated along the surface of a 19 μm radius fiber following [3,4] by the local nanoscale variation of the effective fiber radius with a focused CO_2 laser beam. The introduced effective radius variation is measured using the microfiber scanning method [22, 23]. In this method, a biconical optical fiber taper having a micron diameter waist is positioned normal to the test SF, as e.g., WG_1 in Fig. 1. The waist of the taper is translated along the SF and touches it periodically at the contact points where the transmission spectra of the taper are measured. These spectra are used for the determination of the SF radius variation. In our experiments, the resonant transmission amplitude spectra are determined with the Luna Optical Vector Analyzer (wavelength resolution 1.3 pm). The experimental data is taken along the SF at contact points spaced by 2 μm. In previous publications [3,4], the effective radius variation of similar microresonators was approximately determined by enveloping the spectral resonances and rescaling the wavelength variation $\Delta\lambda$ to radius variation Δr with the relation $\Delta\lambda / \lambda_{res} = \Delta r / r_0$. However, the theory enabling the accurate determination of the effective radius variation and the WG/SF coupling parameters from the experimental data has not been developed.

It is shown in this Section that the Schrödinger Eq. (2) and Eq. (4) for the transmission amplitude allow the accurate determination of the characteristics of a SNAP device from the experimental data. To this end, the effective radius variation of the SF is determined by fitting the spectrum found by the numerical solution of the Schrödinger Eq. (2) to the experimental

#174047 - $15.00 USD Received 8 Aug 2012; revised 11 Sep 2012; accepted 12 Sep 2012; published 17 Sep 2012

spectrum. Two examples are considered: a single SNAP bottle microresonator and a chain of 10 coupled microresonators.

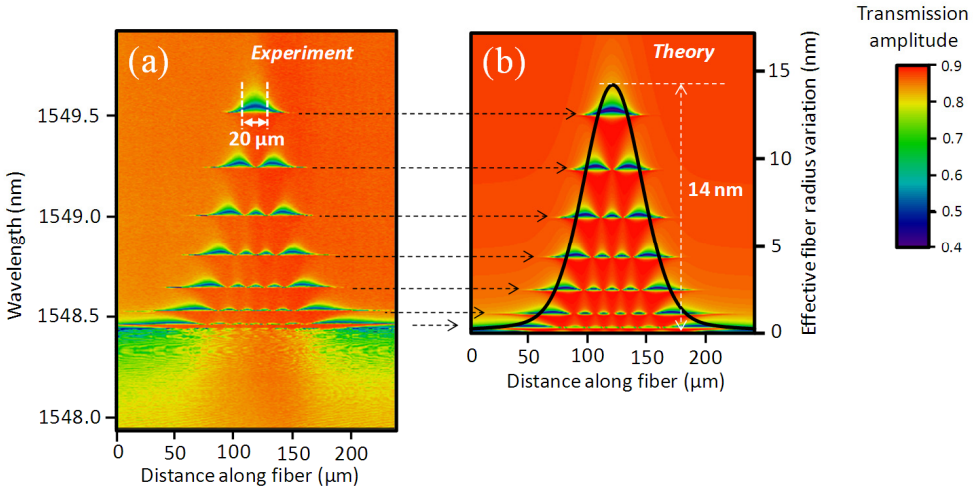

Fig. 5. (a) – The surface plot of the experimentally measured resonant transmission amplitude through the microfiber scanned along the SNAP bottle resonator with 2 μm steps. (b) – Surface plot of the theoretically calculated transmission amplitude fitting the experimental data of Fig. 5(a).

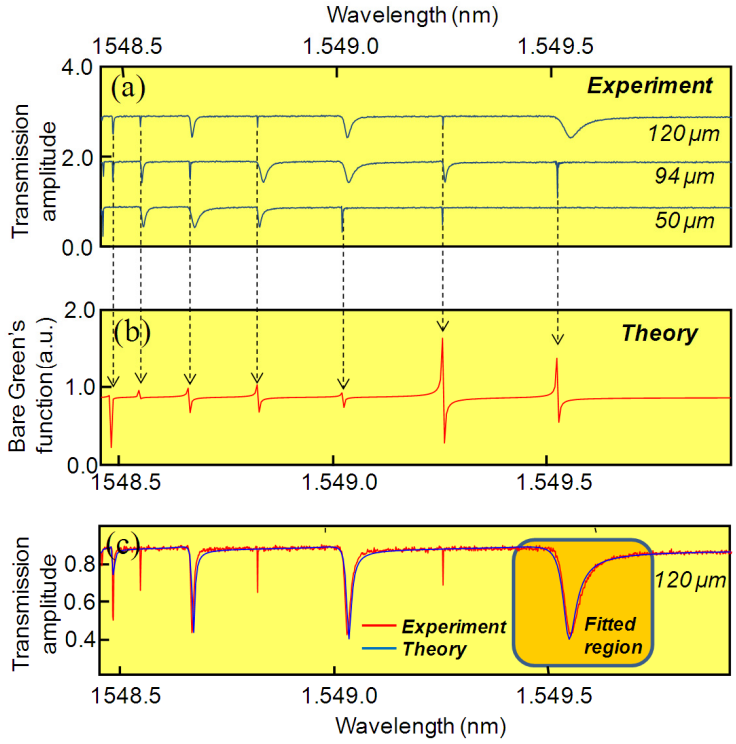

Fig. 6. (a) – The experimental transmission amplitudes of the bottle microresonator from Fig. 5(a) measured at the axial microfiber positions 50 μm, 94 μm, and 120 μm. (b) – The bare Green's function calculated with the radius dependence defined by Eq. (27) fitting narrow experimental resonances in Fig. 6(a). (c) – Fitting the experimental transmission amplitude at axial position 120 μm.

#174047 - $15.00 USD Received 8 Aug 2012; revised 11 Sep 2012; accepted 12 Sep 2012; published 17 Sep 2012

In the first experiment, a single SNAP bottle resonator is fabricated and investigated. This microresonator was created by a single exposure of the focused CO_2 laser beam. The surface plot of the resonant transmission amplitudes for this microresonator is shown in Fig. 5(a). It is seen that the spectral resonances are broadened and shifted due to coupling to the microfiber. Therefore, the actual spectrum of the uncoupled bottle resonator is determined in the regions where the coupling is minimized, i.e., near nodes of the field and in evanescent regions. The set of transmission amplitudes, which correspond to the microfiber positions 50 μm, 94 μm, and 120 μm and jointly contain all of such narrow resonances indicated by dashed arrows, are shown in Fig. 6(a). These resonances are numerically fitted to the eigenvalues of the Schrödinger Eq. (2) where the effective fiber radius variation of the SNAP bottle microresonator is parameterized as a sum of Gaussian and Lorentzian shapes:

$$\Delta r_{eff}(z) = \Delta r_0 \left[\exp\left(-\frac{(z-z_0)^2}{\zeta^2} \right) + \frac{\varepsilon}{1+[(z-z_0)^2/\zeta^2]} \right] \tag{25}$$

The eigenvalues of Eq. (2) are found as the singularities of the bare Green's function $G(\lambda, z_1, z_1)$ where z_1 is taken close to the center of symmetry of $\Delta r_{eff}(z)$. The result of fitting yields

$$\Delta r_0 = 14.1\,\text{nm}, \qquad \zeta = 10.9\,\mu\text{m}, \qquad z_0 = 120\,\mu\text{m}, \qquad \varepsilon = 0.22, \tag{26}$$

and completely determines the effective radius variation, Eq. (25). The theoretical wavelength eigenvalues calculated with these parameters for $G(\lambda, 130\mu\text{m}, 130\mu\text{m})$ and experimental eigenvalues found from Fig. 6(a) are compared in Fig. 6(b). Next, parameters $S_{11}^{(0)}$, $|C_1|^2$, and D_1 of the transmission amplitude $S_{11}(\lambda)$, Eq. (8), are determined by substitution of the bare Green's function $G(\lambda, z_1, z_1)$ calculated for the radius variation determined by Eqs. (25) and (26) into Eq. (8) and fitting it to the experimental transmission amplitude at $z = 120\,\mu$m. The result of fitting shown in Fig. 6(c) performed in the vicinity of the fundamental resonance (darken area in Fig. 6(c)) yields:

$$S_{11}^{(0)} = 0.879 - 0.084i, \qquad |C_1|^2 = 0.026\,\mu\text{m}^{-1}, \qquad D_1 = 0.022 + 0.02i\,\mu\text{m}^{-1}. \tag{27}$$

As expected, these values satisfy the conditions of Eqs. (10) and (11) following from energy conservation. Note that the absence of several resonant peaks on the theoretical spectral dependence in Fig. 6(c) is explained by the fact that this spectrum corresponds to the microresonator plane of symmetry. At this plane, the antisymmetric axial modes are dark and do not show up on the spectrum. On the other hand, these resonances are clearly seen at the theoretical spectrum in Fig. 6(b). Finally, the calculation of the transmission amplitude, Eq. (8), with parameters given by Eq. (27) and the radius variation given by Eqs. (25) and (26) yields excellent correspondence between the experimental data shown in Fig. 5(a) and the theoretical calculations shown in Fig. 5(b). In addition there is an agreement between the surface plots of the Gaussian mode transmission amplitude shown in Fig. 2(f) with those in Fig. 5 in the vicinity of the fundamental mode wavelength (~1549.5 nm).

In the second experiment, a chain of 10 coupled SNAP microresonators illustrated in the inset of Fig. 7 is fabricated and investigated. This chain was created by ten successive exposures of the focused CO_2 laser beam spaced by 50 μm. The surface plot of the resonant transmission amplitudes for this chain is shown in Fig. 7(a). It is seen that, due to mutual coupling, the fundamental modes of microresonators form a transmission band (outlined by a dashed line) separated from other modes by a bandgap. The magnified surface plot of the fundamental transmission band is shown in Fig. 7(b). The observed spectral plots can be described theoretically by approximating the effective fiber radius variation as:

#174047 - $15.00 USD Received 8 Aug 2012; revised 11 Sep 2012; accepted 12 Sep 2012; published 17 Sep 2012

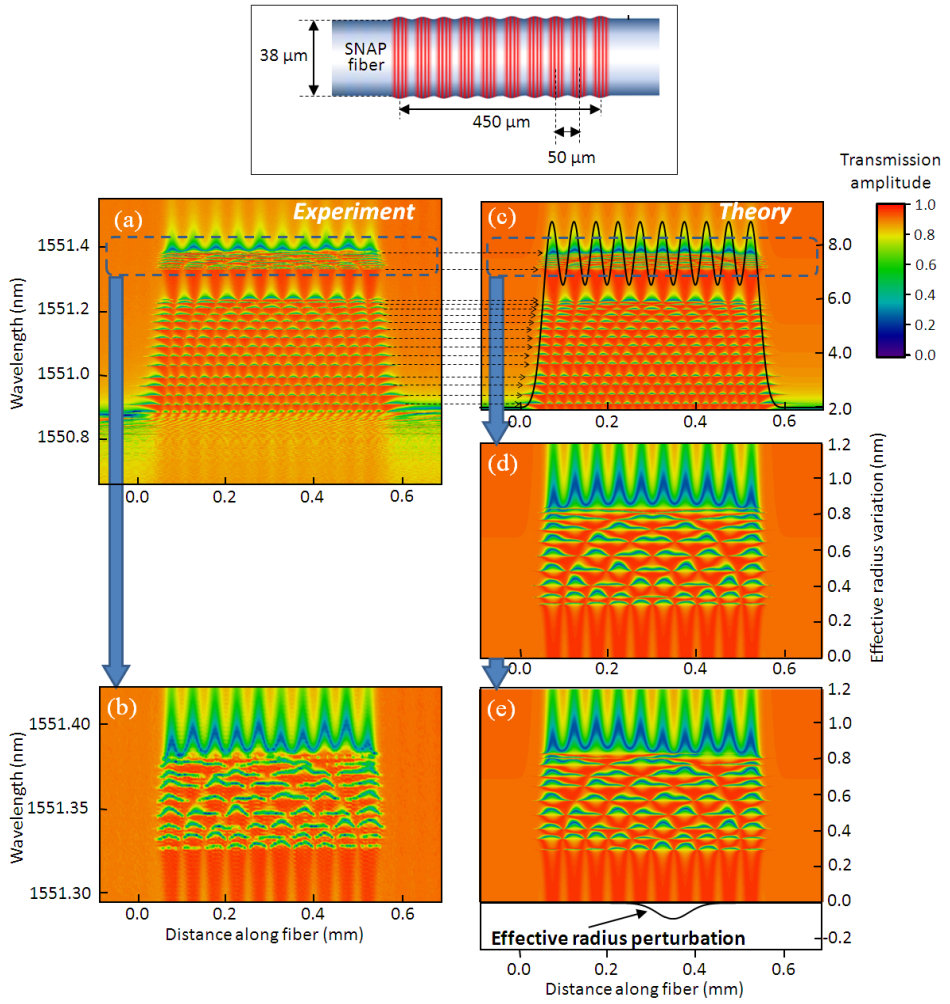

Fig. 7. (a) – The surface plot of the experimentally measured resonant transmission amplitude through the microfiber scanned along the chain of 10 SNAP microresonators with 2 µm steps. (b) – Surface plot of Fig. 7(a) magnified in the region of the fundamental transmission band. (c) – Surface plot of the theoretically calculated transmission amplitude fitting the experimental data of Fig. 7(a). (d) – Surface plot of Fig. 7(c) magnified in the region of the fundamental transmission band. (e) – Surface plot of Fig. 7(d) perturbed by the effective radius variation shown at the bottom of Fig. 7(e).

$$\Delta r_{eff}(z) = \Delta r_0 \begin{cases} \exp\left(-z^2/\zeta^2\right), & z<0, \\ \dfrac{a^2}{2\pi^2\zeta^2}\left(\cos\left(2\pi z/a\right)-1\right)+1, & 0<z<Na, \\ \exp\left\{-[z-(N-1)a]^2/\zeta^2\right\}, & z>(N-1)a, \end{cases} \tag{28}$$

where $a = 50\,\mu$m is the microresonator spacing, $N = 10$ is the number of microresonators, and parameters Δr_0 and ζ are the fitting parameters. Equation (28) describes periodic oscillations of the effective radius variation in the exposed region. Parameters Δr_0 and ζ are determined by fitting the experimental distribution of higher-order resonances below the bandgap and also the bandgap position in Fig. 7(a). The fitting, which is performed similar to

#174047 - $15.00 USD Received 8 Aug 2012; revised 11 Sep 2012; accepted 12 Sep 2012; published 17 Sep 2012

the previous example (see dashed arrows connecting the experimental and theoretical spectra in Fig. 7(a) and 7(c)), yields:

$$\Delta r_0 = 6.9\,\text{nm}, \qquad \zeta = 19.4\,\mu\text{m}, \qquad a = 50\mu\text{m}, \qquad N = 10. \tag{29}$$

The resultant effective radius variation is shown in Fig. 7(c). The parameters of the transmission amplitude distribution in Fig. 7(c) are:

$$S_{11}^{(0)} = 0.83 - 0.15i, \qquad |C_1|^2 = 0.028\,\mu\text{m}^{-1}, \qquad D_1 = 0.022 + 0.026i\,\mu\text{m}^{-1}. \tag{30}$$

The magnified distribution of this plot near the region of fundamental transmission band is shown in Fig. 7(d). Notice a remarkable agreement between the fine features of this plot and of the experimental plot shown in Fig. 7(b). A small deviation of the experimental spectra in Fig. 7(b) from the theoretical distribution in Fig. 7(d) can be approximately taken into account by perturbing $\Delta r_{eff}(z)$ with a Gaussian radius variation $\delta r_{eff}(z) = \delta r_0 \exp[-(z - z_0)^2 / \zeta_0^2]$ with $\delta r_0 = 0.1\,\text{nm}$, $z_0 = 350\,\mu\text{m}$, and $\zeta_0 = 100\,\mu\text{m}$, shown at the bottom of Fig. 7(e). The small angstrom amplitude of $\delta r_{eff}(z)$ allows us to suggest an angstrom precision in the fabrication of this microresonator chain.

7. Discussion and summary

The theory developed in this paper can be directly applied both to modeling of SNAP devices and to their evaluation from the experimental data. The basic assumptions of this theory following from the experimental conditions are (a) adiabatic separation of variables and reduction of a 3D problem for the bare Green's function to a 1D Schrödinger equation and (b) the axial dimension of SF/waveguide coupling region being much smaller than the characteristic axial wavelength of this equation. The latter assumption allows us to arrive at the 1D Schrödinger equation for the renormalized Green's function of the SNAP device, Eq. (4). In this equation, coupling to a waveguide is described by a short-range potential characterized by a complex-valued coupling constant. As a result, the transmission amplitudes of a SNAP device coupled to N waveguides are expressed through the values of the bare Green's function calculated at the waveguide positions and $3N$ complex constants $S_{1n}^{(0)}$, C_n, and D_n. General inequality relations between these parameters following from energy conservation are obtained. The developed theory is applied to the investigation of the simplest SNAP devices: a separated resonance state, a uniform fiber, and a bottle microresonator coupled to one or two waveguides. The cases of ideal (lossless) coupling as well as lossy coupling to waveguides are considered. It is found that these simplest devices can exhibit quite complex resonance spectra depending on the values of the coupling parameters. The problem of the theoretical determination of constants $S_{1n}^{(0)}$, C_n, and D_n through the SF and waveguide parameters is not addressed in this paper since it is often more straightforward and accurate to determine these values experimentally. As an example, these constants and the SF radius variation are determined from the experimental data of a SNAP bottle microresonator coupled to a single waveguide. In this case, the excellent agreement between the theory and the experiment is demonstrated. Generally, it is quite interesting to determine the parameters $S_{1n}^{(0)}$, C_n, and D_n theoretically and, in particular, to get a better understanding of how they are related to each other. The developed theory provides a way to investigation of the transmission properties of SNAP devices with a complex variation of the SF radius, e.g., chains of coupled microresonators considered in Section 6, including the optimization of coupling between microresonators and waveguides [16] to achieve the required filtering and group delay characteristics.

#174047 - $15.00 USD Received 8 Aug 2012; revised 11 Sep 2012; accepted 12 Sep 2012; published 17 Sep 2012

Appendix 1

Transmission amplitude of a SNAP device

The WGMs in the SF coupled to waveguides can be found by adiabatic separation of variables, similar to Eq. (1):

$$U^{(ren)}_{m,p,q}(\mathbf{r}) = \Psi^{(ren)}_{m,p,q}(z)\Xi_{m,p}(\rho)\exp(im\varphi) \tag{A1.1}$$

where function $\Psi^{(ren)}_{m,p,q}(z)$ satisfied Eq. (4) and $\mathbf{r} = (z,\rho,\varphi)$ is expressed in cylindrical coordinates. The Green's function is constructed from these solutions as

$$\mathcal{G}(\lambda,\mathbf{r}_1,\mathbf{r}_2) = \sum_{m,p,q}\frac{U^{(ren)}_{m,p,q}(\mathbf{r}_1)U^{(ren)*}_{m,p,q}(\mathbf{r}_2)}{E(\lambda)-E_{m,p,q}} \tag{A1.2}$$

Using Eq. (A1.1) we can summarize Eq. (A1.2) over q,

$$\mathcal{G}(\lambda,\mathbf{r}_1,\mathbf{r}_2) = \sum_{m,p}G^{(ren)}_{m,p}(\lambda,z_1,z_2)\Xi_{m,p}(\rho_1)\Xi_{m,p}(\rho_2)\exp[im(\varphi_1-\varphi_2)], \tag{A1.3}$$

where $G^{(ren)}_{m,p}(\lambda,z_1,z_2)$ is the renormalized Green's function of Eq. (4) (see also Appendix A2 in [2]).

We define $\chi_n(\mathbf{r})$ as the wave propagating along the single mode waveguide WG_n in the absence of SF when the waveguides do not couple to each other. The SF is introduced with a potential V(**r**) so that the T-matrix, which determines the inter-waveguide coupling due to the presence of the SF, is expressed through the Green's function of Eq. (A1.2) as $\mathcal{T} = \mathcal{V} + \mathcal{V}\mathcal{G}\mathcal{V}$ [24]. Then, the transmission amplitudes between the waveguide modes are determined by the elements of the S-matrix [24]:

$$\mathcal{S} = 1 - i\mathcal{T} = 1 - i(\mathcal{V} + \mathcal{V}\mathcal{G}\mathcal{V}) \tag{A1.4}$$

From Eq. (A1.4), for the amplitude of the direct transmission through the waveguide WG_1 we have:

$$S_{11}(\lambda) = 1 - i\int d\mathbf{r}_1 \,|\,\chi_1(\mathbf{r}_1)\,|^2\,\mathcal{V}(\mathbf{r}_1) - i\int d\mathbf{r}_1 d\mathbf{r}_2 \chi_1(\mathbf{r}_1)\mathcal{V}(\mathbf{r}_1)\mathcal{G}(\lambda,\mathbf{r}_1,\mathbf{r}_2)\mathcal{V}(\mathbf{r}_2)\chi_1^*(\mathbf{r}_2) \tag{A1.5}$$

In the vicinity of the resonance $E(\lambda_{m_0,p_0}) = E_{m_0,p_0}$, only one term in Eq. (A1.3) with $m = m_0$ and $p = p_0$ has resonance behavior, while all others are slow functions of E which can be set to constants. In SNAP, the axial size of the waveguide/SF coupling area is small compared to the axial wavelength (i.e., to the characteristic axial variation length of the Green's function $G^{(ren)}_{m,p}(\lambda,z_1,z_2)$). For this reason, the coordinates z_j in Eq. (A1.5) can be set equal to the axial coordinate of WG_1, z_1, and $G^{(ren)}_{m,p}(\lambda,z_1,z_1)$ can be factored out of the integral. Thus, substitution of Eq. (A1.3) into Eq. (A1.5) yields:

$$\begin{aligned} &S_{11}(\lambda) = S^{(0)}_{11} - i\,|\,C_1\,|^2\,G^{(ren)}_{m_0,p_0}(\lambda,z_1,z_1), \\ &C_1 = \int d\mathbf{r}\chi_1(\mathbf{r})\mathcal{V}(\mathbf{r})\Xi_{m_0,p_0}(\rho)\exp(im_0\varphi). \end{aligned} \tag{A1.6}$$

Here $S^{(0)}_{11}$ includes contribution of non-resonant terms. If this contribution is negligible, e.g., for very small "ideal" [20] waveguide/SF coupling, we have $S^{(0)}_{11} = 1$, while generally

#174047 - $15.00 USD Received 8 Aug 2012; revised 11 Sep 2012; accepted 12 Sep 2012; published 17 Sep 2012

$|S_{11}^{(0)}|<1$. It is important that, due to its non-resonant nature, $S_{11}^{(0)}$ is constant in the considered wavelength interval with good accuracy.

Similarly to Eq. (A1.6), the amplitude of transmission from WG_1 to WG_n is

$$\begin{aligned} &S_{1n}(\lambda) = S_{1n}^{(0)} - iC_1C_n^* G_{m_0,p_0}^{(ren)}(\lambda, z_1, z_n), \\ &C_n = \int d\mathbf{r}\chi_n(\mathbf{r})\mathcal{V}(\mathbf{r})\Xi_{m_0,p_0}(\rho)\exp(im_0\varphi), \end{aligned} \tag{A1.7}$$

where constant $S_{1m}^{(0)}$ is the non-resonant component. In the main text, the indices m_0 and p_0 are omitted and the notation $\bar{G}(\lambda, z_1, z_n) = G_{m_0,p_0}^{(ren)}(\lambda, z_1, z_n)$ is used.

Appendix 2

Calculation of the Green's functions

The bare Green's function of Eq. (2) is defined through the solutions of Eq. (2) $\Psi_1(\lambda, z)$ and $\Psi_2(\lambda, z)$, which satisfy the boundary conditions in the left-hand side and in the right-hand sides, respectively, and have the unity Wronskian,

$$\Psi_{1z}(\lambda, z)\Psi_2(\lambda, z) - \Psi_1(\lambda, z)\Psi_{2z}(\lambda, z) = 1, \tag{A2.1}$$

as

$$G(\lambda, z_1, z_2) = \begin{cases} \Psi_1(\lambda, z_1)\Psi_2(\lambda, z_2) & z_1 > z_2 \\ \Psi_1(\lambda, z_2)\Psi_2(\lambda, z_1) & z_1 < z_2 \end{cases}. \tag{A2.2}$$

The renormalized Green's function of Eq. (4) is expressed through the linear combination of the same functions, $K_{1n}\Psi_1(\lambda, z) + K_{2n}\Psi_2(\lambda, z)$, where the coefficients K_{1n} and K_{2n} correspond to the axial interval $z_n < z < z_{n+1}$. These coefficients are determined by $2n$ matching conditions at the points of coupling z_n:

$$\begin{aligned} &\bar{G}(\lambda, z, z_n)\Big|_{z \searrow z_n} - \bar{G}(\lambda, z, z_n)\Big|_{z \swarrow z_n} = 0, \qquad n = 1, 2, ..., N \\ &\bar{G}_z(\lambda, z, z_1)\Big|_{z \searrow z_1} - \bar{G}_z(\lambda, z, z_1)\Big|_{z \swarrow z_1} = 1 + iD_1\bar{G}(\lambda, z, z_1) \\ &\bar{G}_z(\lambda, z, z_1)\Big|_{z \searrow z_n} - \bar{G}_z(\lambda, z, z_1)\Big|_{z \swarrow z_n} = iD_n\bar{G}(\lambda, z_2, z_1), \qquad n = 2, 3, ...N \end{aligned} \tag{A2.3}$$

where the tilted arrow in $z \searrow z_n$ and $z \nearrow z_n$ means the limit to point z_n for $z > z_n$ and $z < z_n$, respectively. It is assumed in Eqs. (A2.3) that WG_1 is the only input and output waveguide, while all others are output only waveguides.

From Eqs. (A2.3), for a SNAP device with a single waveguide WG_1, $N = 1$, the renormalized Green's function is defined by Eq. (7).

For a SNAP device with two waveguides WG_1 and WG_2, $N = 2$, the continuity condition (the first equation in Eqs. (A2.3)) is incorporated for the renormalized Green's function in the form:

$$\bar{G}(\lambda, z, z_1) = \begin{cases} [A_1\Psi_1(\lambda, z_1) + A_2\Psi_2(\lambda, z_1)]\Psi_1(\lambda, z)\Psi_2(\lambda, z_2), & z < z_1, \\ [A_1\Psi_1(\lambda, z) + A_2\Psi_2(\lambda, z)]\Psi_1(\lambda, z_1)\Psi_2(\lambda, z_2), & z_1 < z < z_2, \\ [A_1\Psi_1(\lambda, z_2) + A_2\Psi_2(\lambda, z_2)]\Psi_1(\lambda, z_1)\Psi_2(\lambda, z), & z > z_2. \end{cases} \tag{A2.4}$$

#174047 - $15.00 USD Received 8 Aug 2012; revised 11 Sep 2012; accepted 12 Sep 2012; published 17 Sep 2012

Then Eqs. (A2.3) are reduced to the system of two linear equations for the coefficients A_1 and A_2. The solution of this system yields Eqs. (18) and (19) for the renormalized Green's function.

Appendix 3

Limitations on the transmission amplitude and coupling parameters

For an inactive SF coupled to a single waveguide WG_1, the conservation of energy requires $|S_{11}(\lambda)|<1$. This inequality applied to Eq. (8) yields:

$$\Lambda_0 + 2\,\mathrm{Re}(\Lambda_1 G) + \Lambda_0^{-1}(|\Lambda_1|^2 - |C_1|^4)|G|^2 > 0 \tag{A3.1}$$

where, for brevity, $G = G(\lambda, z_1, z_1)$ and

$$\begin{aligned} \Lambda_0 &= 1 - |S_{11}^{(0)}|^2, \\ \Lambda_1 &= i|C_1|^2 (S_{11}^{(0)})^* - i\Lambda_0 D_1. \end{aligned} \tag{A3.2}$$

The Green's function of an inactive SF obeys the general condition $\mathrm{Im}(G)<0$ [12], while there are no formal restrictions on $\mathrm{Re}(G)$. Thus, Eq. (A3.1) should be satisfied for all complex values of G with $\mathrm{Im}(G)<0$.

Let us start with the case $\mathrm{Im}(G)=0$. Then Eq. (A2.1) is simplified to

$$\Lambda_0 + 2\,\mathrm{Re}\,\Lambda_1\,\mathrm{Re}\,G + \Lambda_0^{-1}(|\Lambda_1|^2 - |C_1|^4)(\mathrm{Re}\,G)^2 > 0, \tag{A3.3}$$

which should be valid for all $-\infty < \mathrm{Re}(G) < \infty$. This condition is equivalent to

$$\Lambda_0 > 0, \tag{A3.4}$$

$$|\,\mathrm{Im}\,\Lambda_1| \geq |C_1|^2. \tag{A3.5}$$

The minimum value of the left-hand side of Eq. (A3.3) is achieved for $\mathrm{Re}\,G = -\Lambda_0\,\mathrm{Re}(\Lambda_1)(|\Lambda_1|^2 - |C_1|^4)^{-1}$ and is equal to

$$\Xi_0 = \Lambda_0\left(1 - \frac{\mathrm{Re}(\Lambda_1)}{|\Lambda_1|^2 - |C_1|^4}\right). \tag{A3.6}$$

Generally, Eq. (A3.1) is satisfied under the conditions determined by Eq. (A3.4) and Eq. (A3.5) and

$$\Xi_0 - 2\,\mathrm{Im}\,\Lambda_1\,\mathrm{Im}\,G + \Lambda_0^{-1}(|\Lambda_1|^2 - |C_1|^4)(\mathrm{Im}\,G)^2 > 0 \tag{A3.7}$$

for all $\mathrm{Im}(G) \leq 0$. Eq. (A3.7) is equivalent to the condition

$$\mathrm{Im}\,\Lambda_1 > |C_1|^2, \tag{A3.8}$$

which is stronger than Eq. (A3.5).

To summarize, the inequality $|S_{11}(\lambda)|<1$ following from the conservation of energy imposes a limitation on parameters C_1, D_1, and $S_{11}^{(0)}$ of the transmission amplitude $S_{11}(\lambda)$, which are determined by Eqs. (A3.4) and (A3.8) equivalent to Eqs. (10) and (11), respectively.

#174047 - $15.00 USD Received 8 Aug 2012; revised 11 Sep 2012; accepted 12 Sep 2012; published 17 Sep 2012

Acknowledgments

The author is grateful to Y. Dulashko for assisting in the experiments and to D. J. DiGiovanni and J. M. Fini for useful discussions.

#174047 - $15.00 USD Received 8 Aug 2012; revised 11 Sep 2012; accepted 12 Sep 2012; published 17 Sep 2012